CO_2 capture by Supported Ionic Liquid Phase (SILP): Highlighting the role of the particle size

Ruben Santiago, Jesus Lemus, Daniel Hospital-Benito, Cristian Moya, Jorge Bedia, Noelia Alonso-Morales, Juan J. Rodriguez and Jose Palomar*

Chemical Engineering Department. C/ Francisco Tomás y Valiente 7. Universidad Autónoma de Madrid. 28049 Madrid. Spain

*E-mail corresponding author: pepe.palomar@uam.es

Keywords: CO_2 capture; Ionic Liquids; SILP; Fixed-bed, Particle Size; Kinetics.

Abstract

CO_2 capture by fixed-bed sorption has been evaluated using Supported Ionic Liquids Phase (SILP) based on the ionic liquid 1-butyl-3-methylimidazolium acetate ([bmim][acetate]). The SILP sorbent was prepared with three remarkably different mean particle size and characterized by porous texture, morphology, thermal stability and elemental composition. The thermodynamics and kinetics of the CO_2 capture process have been studied, testing the effects of SILP particle size, sorption temperature, gas flow rate and CO_2 partial pressure. The CO_2 sorption isotherms at different temperatures were obtained by gravimetric measurements, revealing that the equilibrium sorption capacity is only due to the IL incorporated on the silica support of SILP. The experimental isotherms were successfully fitted to Langmuir-Freundlich model. Fixed-bed experiments of CO_2 capture were carried out to evaluate the performance of the SILP sorbents at different operating conditions. All the breakthrough curves were well described by a linear driving force model. The obtained kinetic coefficients revealed that the CO_2 sorption rate in fixed-bed linearly increases when decreasing the SILP particle size and increasing the operating temperature. Higher CO_2 partial pressure in the inlet gas stream led to faster mass transfer rate, affecting both the mass transfer driving force and kinetic coefficient. Aspen Adsorption simulator was successfully applied to model the fixed bed operation, highlighting the role of the particle size on separation efficiency. Simulations results indicate that at very low CO_2 partial pressure chemical absorption is the controlling step, while increasing that partial pressure shifts the regime towards diffusion into the SILP. This methodology will allow designing CO_2 sorption systems based on SILPs that

fulfill the separation requirements at given conditions (CO_2 partial pressure and temperature), minimizing the SILP needs by optimizing the particle size and type of IL.

Introduction

Concerns for climate change owing to anthropogenic emissions of carbon dioxide (CO_2) are now well recognized and have resulted in a number of initiatives to reduce CO_2 emissions [1, 2]. In this sense, carbon capture and storage (CCS) technologies are considered a main strategy, due to their efficiency and relatively low cost [3-5]. Regarding physical absorption, high operating pressures are required and solvents such as glymes mixtures (comprising Selexol® solvent) are widely used [6, 7]. However, these solvents present problems, such as high toxicity, corrosive nature and high volatility resulting in high solvent losses and negative environmental impact [8, 9]. On the other hand, in chemical absorption processes, amines are commonly used, but they are corrosive and suffer degradation, also resulting in high solvent losses, environmental impact and considerable maintenance and operating costs [10, 11]. In order to overcome these disadvantages, ionic liquids (ILs) have awakened great attention due to their unique properties, such as very low vapor pressure, good thermal and chemical stability and high solvent capacity [12-14]. In CO_2 capture, ILs can be applied to uptake CO_2 by either physical [15] or chemical absorption [16]. It is widely reported that CO_2 possesses relatively high solubility in ILs [17]. More recently, it has been suggested that CO_2 capture by chemical absorption seems to be the most convenient strategy for the CO_2 retention with ILs, being acetate-based ILs [18] or Aprotic Heterocyclic Anions-based ILs (AHA) [19] widely used. Nevertheless, they still present some drawbacks mainly due to their limited transport properties. This technical limitation for the practical application of ILs in CO_2 capture is a consequence of their high viscosity (comparing with other solvents as amine solutions) [20], which can even increase in some cases upon reaction with CO_2 [21]. In fact, some recent works demonstrate that mass transfer controls the rate of CO_2 capture based on ILs [20, 22, 23].

Therefore, novel strategies using ILs are needed in order to overcome those limitations. In this scenario, Supported Ionic Liquid Phase (SILP), consisting of the immobilization of ILs on a solid support, have been proposed as a potential solution [24]. SILP materials are commonly prepared by spreading a film of IL onto the surface of a solid support, mostly consisting of materials with high specific surface area, like activated carbon, zeolite, or silica [25]. It has been demonstrated that the IL immobilization on a porous support drastically increases the gas/liquid contact area, leading to much faster

sorption than with the bulk ionic liquid [26, 27]. In addition, the negligible vapor pressure, large liquid range, and thermal stability of ILs ensure that the solvent is retained on the support in its fluid state even at elevated temperatures; this makes SILP highly suitable for gas separation continuous processes [28]. Recently, our group developed the Encapsulated Ionic Liquids (ENILs), which consist of uploading a large amount of IL inside carbonaceous submicrocapsules [29], being tested in the capture of different gases (NH_3 or CO_2) [30-34]. It was demonstrated that it is possible to overcome the mass transfer limitations (that typically control the absorption rates) in neat ILs by increasing the gas-liquid contact area using ENIL or SILP materials [30-34]. Consequently, in the last years, huge efforts have been addressed to develop novel sorbents based on ILs, which could be used to mitigate the world's CO_2 emissions.

On the other hand, the development of CO_2 capture processes by adsorption in fixed-bed has also attracted the attention of the scientific community, with a wide variety of proposed adsorbents (active carbon, silica or zeolites, among others) [35-38]. In such studies, the particle size of the adsorbent has been a key issue, determining the sorption rate and, consequently, the adsorbent need and the separation efficiency [39-42]. However, to the best of our knowledge, no systematic studies dealing with the CO_2 capture with SILPs of different support particle sizes have been published. In addition, the modelling of the thermodynamics and kinetics of CO_2 sorption in SILPs has still not been explored. This modelling would allow designing the operation by process simulation, which is a key framework for the development of new separation processes based on ILs[20, 32]. In this context, Aspen Adsorption (implemented in the Aspen ONE® suite package) has been successfully used to model experimental breakthrough curves of different adsorbents and, consequently, to perform process analysis to estimate adsorbent loads, column dimensions, operating time, used bed fraction, etc. [43-45].

In this work, the experimental sorption isotherms and breakthrough curves of CO_2 in SILP material were obtained at different operating conditions. Three SILP sorbents have been tested, all based on the IL 1-butyl-3-methylimidazolium acetate supported on silica but with remarkably different particle sizes (difference of three orders of magnitude). They contained almost the same IL loading (~ 40%w/w) and were characterized by N_2 adsorption/desorption at 77 K, SEM microscopy, thermal stability and elemental analysis. The aim of the study is to evaluate and describe the influence of the particle size in both the thermodynamics and kinetics of the process at different

operating conditions. The corresponding equilibrium isotherms were obtained by a gravimetric procedure using a magnetic suspension balance at different sorption temperatures (299 – 333 K) within a CO_2 partial pressures range of 0.3 to 20 bar. The isotherms were well described by the Langmuir-Freundlich model. Then, fixed-bed CO_2 capture experiments using the SILP sorbents -with the three different particle sizes- were carried out at different temperatures, gas flow rates and CO_2 partial pressures. The experimental breakthrough curves were successfully described by a linear driving force model (LDF) with a lumped resistance, which allows estimating the overall kinetic coefficient (k_{MTC}). A relationship of k_{MTC} with the particle radius, sorption temperature and CO_2 partial pressure was found to describe the SILP performance in fixed-bed CO_2 capture. Finally, the resulting thermodynamic and kinetic models were used in Aspen Adsorption to simulate the CO_2 capture operations based on SILP material, allowing to evaluate the remarkable effect of the particle size on the breakthrough curves, depending on the CO_2 partial pressure in the feed stream.

Experimental section

Materials

The silica gel particles of different size ranges (250-500 µm, 63-210 µm and <37 µm), the IL 1-butyl-3-methylimidazolium acetate [bmim][acetate] (> 95% purity) and acetone (> 99.5% purity) were purchased from Sigma Aldrich. Carbon dioxide, nitrogen and helium were supplied by Praxair, Inc., with a minimum purity of 99.999%. In addition, a mixture containing 10,000 ppmv of carbon dioxide in nitrogen was supplied by Praxair Inc, which was used in the fixed-bed runs.

SILP preparation and characterization

The silica particles used as support in the SILP material were used without any treatment, directly from the commercial supplier. The SILPs synthesis was carried out by incipient wetness impregnation [28]. In all cases, 1 g of SiO_2 and its corresponding amount of IL for a nominal load of 40%w/w (maximum load that can be introduced in the SiO_2 by the incipient wetness impregnation method), were mixed with acetone. Prior to the synthesis, the IL was dried and degassed at 333 K under vacuum (10^{-3} mbar) for at least 24 h to ensure a water content bellow 200 ppm. Then, the solution was added dropwise onto the SiO_2 support and remained 1 h at room temperature. After the impregnation, the resulting SILP was dried at 333 K for 24 h. Then, the amount of IL incorporated to the support was checked by elemental analysis. This methodology has been successfully

applied in a previous work of our group [28] showing the homogenous distribution of the IL inside the pores of different supports.

The thermal stability of the SILPs was studied by thermogravimetry, using a TA instrument SDT 650 model. The tests were performed under inert atmosphere (50 NmL/min of N_2) with a heating rate of 10ºC/min up to 600 ºC. The porous texture of both the SiO_2 particles and SILP material was characterized by N_2 adsorption/desorption at 77 K in a TriStar II 3020 (Micromeritics) system after 15 h of previous degassing at 0.1 mbar and 363 K. The surface area was calculated using the BET equation. The CHN content of the samples was checked by elemental analysis in a LECO CHNS-932. The microstructure and morphology of the empty SiO_2 particles was studied by scanning electron microscopy (SEM) allowing to calculate the particle size distribution of each sample. SEM analyses were performed with a Hitachi S-3000N apparatus.

Gravimetric CO_2 sorption measurements

The CO_2 sorption capacity in SILP material (mol_{CO2} /kg_{SILP}) was obtained using a gravimetric high-pressure sorption analyzer (ISOSORP GAS LP-flow, Rubotherm) equipped with a magnetic suspension balance (MSB). The apparatus allows controlling the inlet mass flow (up to 500 NmL/min) with two mass-flow meters (N_2 and CO_2), the sorption temperature (from room to 150 ºC) and the total pressure (from 10^{-6} to 30 bar). The microbalance is able to measure weights up to 10 g, with a precision of 10^{-5} g. Full description of the procedure used in the high-pressure sorption tests can be found elsewhere [15, 31]. In this work, the CO_2 sorption isotherms for the different SILPs were obtained at three different temperatures (299, 314 and 329 K). A typical sorption test, used 100-150 mg of SILP material. First, before each CO_2 sorption test, degasification was accomplished by heating the sample up to 333 K at 10^{-3} mbar residual pressure during 24 h. Then, for gravimetric experiments at 0.3 and 0.5 bar of CO_2 partial pressure, a mixture of CO_2-N_2 (total flow of 100 NmL/min) was used. For gravimetric experiments between 1 and 20 bar of CO_2 partial pressure, pure CO_2 was passed through the sample. The mass increase with time was recorded until the SILP was completely saturated (weight change < 0.02 mg/h) at constant temperature and CO_2 partial pressure. Afterwards, the total pressure was increased progressively up to a maximum value of 20.0 bar of pure CO_2. Lastly, in order to have reliable sorption values, the buoyancy effect caused by the MSB must be corrected. To accomplish this, an inert gas was flowed through the sample prior to the sorption test at different pressures and the testing

temperature. The uncertainties of the MSB are: *u(P)* = 0.01 bar; *u(T)* = 0.1 K; $u(q_e)$ = 0.0001 mol/kg.

Fixed-bed CO_2 sorption experiments

The quartz tube of 6 mm of internal diameter and 15 cm of length containing the fixed-bed (SILP length of 10 cm) was placed in a Microactivity unit (PID Eng&Tech, Spain). The tube is placed inside an oven that allows working at temperatures from room to 773 K. Two mass flow meters (N_2 and mixture of CO_2-N_2) fed the reactor in down-flow direction. The set up consists of a pressure gauge at the gas inlet connected to a pressure valve at the exit of the fixed-bed. In current fixed-bed experiments, the pressure at the gas inlet is fixed at 1 bar. The gas outlet is connected to a gas chromatograph (GC Agilent 7820A) equipped with a 20 m column (PoraPlot U) and a TCD detector. In a typical fixed-bed experiment, the quartz tube was filled with 1.5-2.5 g of fresh SILP (corresponding approximately to 9 cm of bed height depending on the material). A mixture of N_2-CO_2 (10% v/v of CO_2) was passed through the bed at 1 atm of total pressure, until the sorbent was completely saturated. For each sorbent, three different temperatures (303, 318 and 333 K), flow rates (10, 20 and 50 NmL/min) and CO_2 inlet concentrations (2.5, 5 and 10% v/v) were tested, at 1 atm total pressure in all cases. Once the bed was saturated, the furnace temperature was raised up to 333 K and inert gas passed during 2 h to allow complete regeneration of the sorbent. The uncertainties of the fixed-bed are: *u(P)* = 0.1 bar; *u(T)* = 1 K.

Computational details: Aspen Adsorption

Isotherms modelling: Experimental CO_2 isotherms were modeled by using the available estimation module implemented in Aspen Adsorption v10.0 software. Firstly, three different equilibrium models (see Figure S1 in Supplementary Material) were checked to fit the experimental CO_2 isotherms. Langmuir-Freundlich equation (L-F Eq. 1) is shown below and the two others can be found in the Supplementary Material. The gases used (CO_2 and N_2) were selected from the Aspen Properties database, choosing as property package Peng Robinson. It was confirmed that N_2 presents a negligible sorption in our materials [46].

$$w_{CO_2}\left[\frac{mol}{kg}\right] = \frac{IP_1 \cdot IP_2 \cdot p_{CO_2}^{IP_3} \cdot e^{IP_4/T}}{1 + IP_5 \cdot p_{CO_2}^{IP_3} \cdot e^{IP_6/T}} \qquad (1)$$

Where w_{CO2} is the equilibrium CO_2 sorption capacity at each partial pressure; p_{CO2} is the CO_2 partial pressure (bar); *T* is the temperature (K) and IP_1, IP_2, IP_3, IP_4, IP_5 and IP_6 are the fitting parameters of the equation.

Breakthrough curves modelling: The pseudo first order LDF kinetic model has been used to describe mass transfer between the gas and the sorbent. In Aspen Adsorption software, this kinetic model is known as lumped resistance linear (LR Eq. 2).

$$\frac{\partial w_{CO2}}{\partial t} = K_{MTC} \cdot (w_{CO2}{}^{*} - w_{CO2}) \qquad (2)$$

It considers all resistances to mass transfer lumped as a single overall factor, or one mass transfer controlling resistance. The driving force is a function of CO_2 adsorbent capacity. The values of the effective kinetic coefficient (k_{MTC}) were calculated by the Aspen Adsorption's estimation module fitting the experimental breakthrough curves using eq. 2 (named Lumped-Resistance model in the software). To accomplish this, some bed parameters and the operating conditions must be fed to the simulator as input information. That information includes bed size, particle radius, bed and particle porosity, bulk sorbent density and operating conditions (pressure, temperature, inlet molar flow and inlet CO_2 partial pressure) as well as the isotherms parameters (*IP*) obtained after the equilibrium model validation. The following assumptions were made: pressure and gas velocity are constant, bed porosity is uniform, plug flow pattern without effect of axial and radial dispersion and constant temperature.

Modelling CO_2 capture operation: Once the thermodynamic and kinetic models were conveniently defined, Aspen Adsorption was used to scale up the CO_2 capture process in fixed-bed under different conditions to optimize the SILP needs in each case. Since it was possible to describe the k_{MTC} as a function of temperature, particle radius and CO_2 partial pressure, the breakthrough curves were modelled using predicted k_{MTC} values for different SILP particle sizes using the dynamic mode. Table 1 shows the operating conditions employed in these Aspen Adsorption simulations. For more input simulation details, see Table S2 of the Supplementary Information.

Table 1: Fixed bed operating conditions used in Aspen Adsorption.

Bed characteristics	
Height of sorbent bed (m)	2
Internal diameter of column (m)	0.3
Operating conditions	
Inlet molar flow rate (mol_{CO2+N2}/min)	1.12
CO_2 mole fraction	0.005-0.5
Temperature (K)	303-333
Pressure (bar)	1

Results

SILP characterization

Silica particles within three different size ranges were used as supports of SILP material as received from the supplier. Figure 1 shows SEM micrographs of representative samples. In all cases, it is clearly observed a fairly irregular morphology with a narrow size distribution. The highest size sample presents a mean size of about 500 µm, the medium one around 150 µm and the smallest near 9 µm (Figure 2). These significant differences allow checking the behavior in SILPs CO_2 sorption depending on the size of the support.

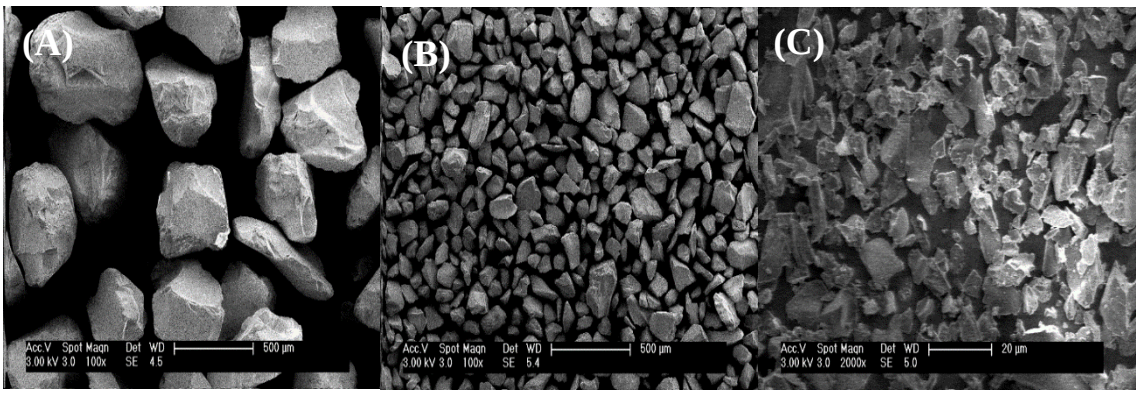

Figure 1: Representative SEM images of the SiO_2 supports of different sizes. Particle size: **(A)** 500 µm; **(B)** 150 µm and **(C)** 9 µm

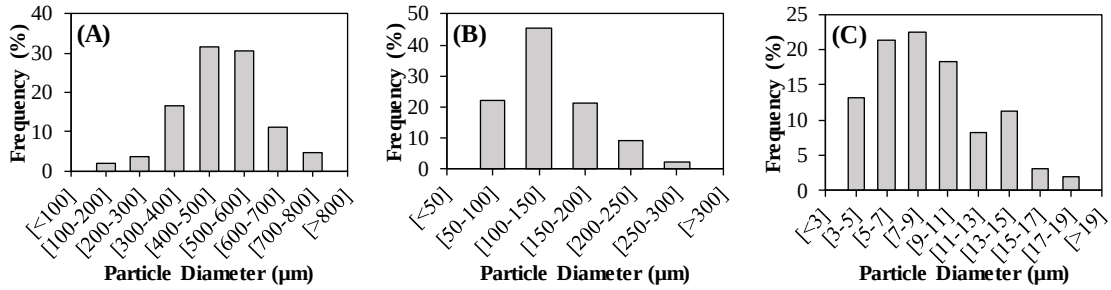

Figure 2: Size distribution of the SiO_2 supports. Mean particle size: **(A)** 500 µm; **(B)** 150 µm and **(C)** 9 µm

TableTable 2 shows the characterization of both the SiO_2 support and SILP material in terms of porous texture, elemental analysis and thermal stability. The 77 K N_2 adsorption-desorption isotherms are given in Figure S1 of the Supplementary Material. The starting supports present similar values of BET surface area in the vicinity of 550 m^2/g. The SILP sorbents synthetized upon incorporation of the IL yielded values below 50 m^2/g, which means that the IL fills most of the support pores. The CHN analysis serves to assess the amount of IL on the support from the %N (only present in the imidazolium cation), as demonstrated in previous works [28, 29]. As expected, the CHN content of the empty SiO_2 particles is close to zero (Table 2) and once the IL was incorporated, the elemental analysis reflects that inclusion. In all cases, IL loading onto SILP material was varied between 37-39%, which allows comparing their performance with nearly the same composition but significantly different particle size. Lastly, the thermal stability of these materials was proved by TGA. The corresponding profiles are given in Figure S2 of Supplementary Information. The SiO_2 particles show no weight loss until at least 600 ºC, while for the SILPs, the mass decay can be attributed to the IL component. The amount of IL on the SILPs from TGA measurements was between 37-39%, in agreement with the results obtained from the elemental analysis.

Table 2: Characterization of SiO_2 supports and SILP material of different particle size

		SiO_2			**SILP**		
		9 µm	150 µm	500 µm	9 µm	150 µm	500 µm
A_{BET}	(m^2/g)	555.5	541.9	588.0	28	28	53
EA	%C	0.01	0.01	0.01	23.1	22.6	21.8
	%H	0.98	1.00	0.99	4.3	4.2	4.0
	%N	0.01	0.01	0.01	5.4	5.2	5.1
%IL	EA	-	-	-	37.9	36.7	36.6
	TGA	-	-	-	40.6	38.4	37.4
T_{DTGA}	(K)	stable until 873K			510.1	510.1	510.1

CO_2 sorption by gravimetric measurements

The thermodynamic (equilibrium) behavior of each SILP in CO_2 capture was first tested by gravimetric measurements. Figure 3 shows the CO_2 sorption isotherms at three different temperatures. Figure S3 and S4 of Supplementary Information compare the CO_2 sorption by the SILPs, the neat IL [bmim][acetate] and the empty SiO_2. It was defined the CO_2 sorption capacity per mass of IL, confirming that the only contribution to CO_2 uptake is due to the IL, in good agreement with previously tested SILP or ENIL materials [29-34]. In fact, the CO_2 uptake at the same temperature is quite similar for the three SILP sorbents, independently of the particle size of the support, since the IL load is also fairly similar (37-39 %). This result is consistent with the dramatic decrease of BET surface area, which confirms the almost complete filling of the SiO_2 pores by the IL [28, 29]. Therefore, it can be concluded that the CO_2 capture by the SILPs is determined by the CO_2 absorption in the IL. The shape of the curves is indicative of dominant chemical absorption, as described in a previous work for the CO_2-[bmim][acetate] system [31]. This fact has been reported in previous works with this and other ILs that chemically retain

CO_2 [30, 31, 33]. Given the great performance of the SILP at low CO_2 partial pressures, we worked within that range in the fixed-bed experiments. As can be seen, the equilibrium data (experimental points) fit very well the Langmuir-Freundlich model (red lines), with $R^2 > 0.99$ in all cases. This model describes the CO_2-SILP equilibrium better than the Langmuir and Freundlich equations, confirming the occurrence of chemical and physical absorption of CO_2 in the IL within the range of CO_2 partial pressure tested, both of them considered in the L-F model. The values of the fitting parameters are collected in Table 3.

Table 3: Fitting parameters of Langmuir-Freundlich model for each temperature and SILP material

Model	**Parameter**	**SILP-500 µm**			**SILP-150 µm**			**SILP-9 µm**		
Langmuir-Freundlich	***T* (K)**	299	314	329	299	314	329	299	314	329
	IP_1	$1.23 \cdot 10^{-3}$			$1.18 \cdot 10^{-3}$			$4.91 \cdot 10^{-4}$		
	IP_2	$1.23 \cdot 10^{-3}$			$1.26 \cdot 10^{-3}$			$1.65 \cdot 10^{-3}$		
	IP_3	0.2326			0.1254			0.1272		
	IP_4	1587.73			1529.43			1778.91		
	IP_5	-1.73			-0.6701			-1.89		
	IP_6	-551.44			-85.12			-428.27		
	R^2*	0.999	0.999	0.997	0.999	0.998	0.999	0.998	0.998	0.992
	sd*	0.015	0.014	0.021	0.013	0.013	0.010	0.020	0.018	0.033

*Statistic parameters calculated comparing experimental and calculated equilibrium data: R^2: square regression coefficient; ***sd***: standard deviation

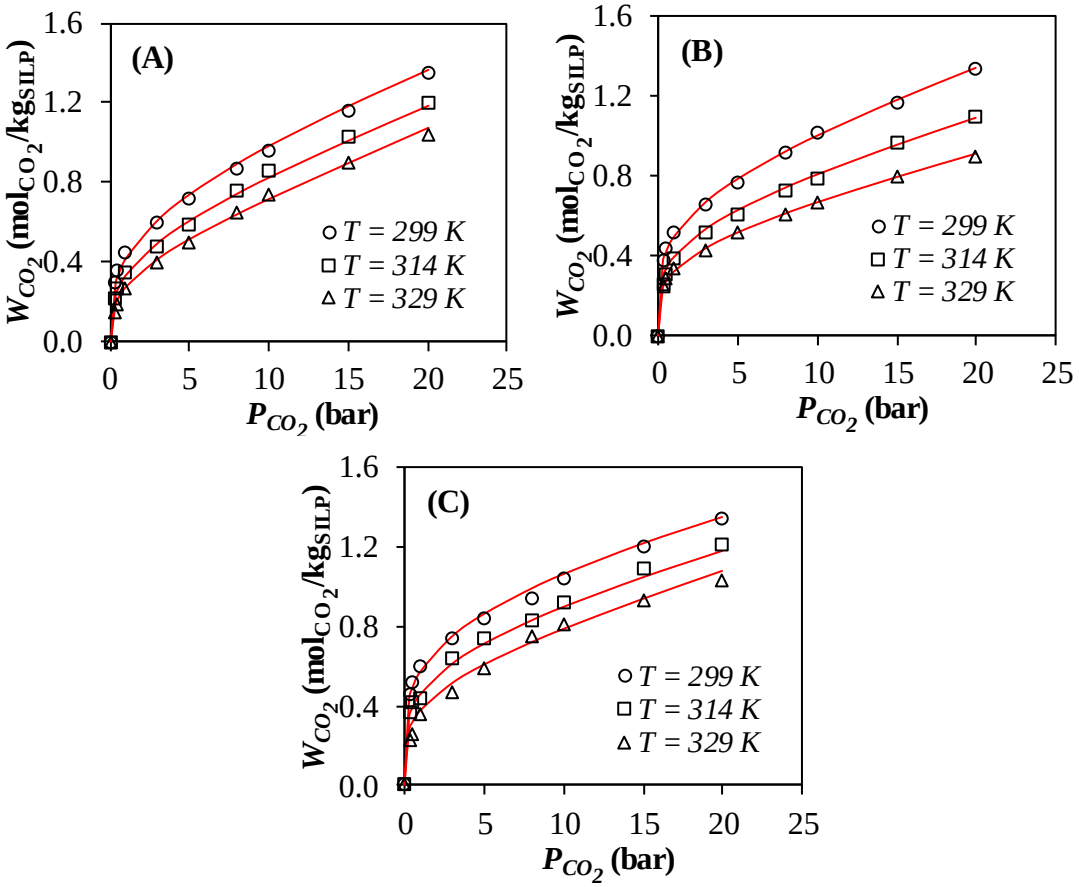

Figure 3: CO_2 isotherms of the three SILP sorbents with different mean particle size. **(A)** 500 µm; **(B)** 150 µm and **(C)** 9 µm.

Fixed-bed experiments

Potential full-scale application of SILP sorbents requires learning on its performance in fixed-bed, where the effects of different variables, such as SILP particle size, temperature, gas flow rate and CO_2 partial pressure need to be evaluated.

The three SILP sorbents with different particle size were first tested at 0.05 bar of CO_2 inlet partial pressure, sorption temperatures of 303, 318 and 333 K and 10 NmL/min of total gas flow. The results are depicted in Figure 4, showing that the LDF model fits very well the experimental data ($R^2 > 0.99$) in all cases. The breakthrough time increases at decreasing temperature, consistently with the higher sorption capacity according the equilibrium curves of Figure 3.

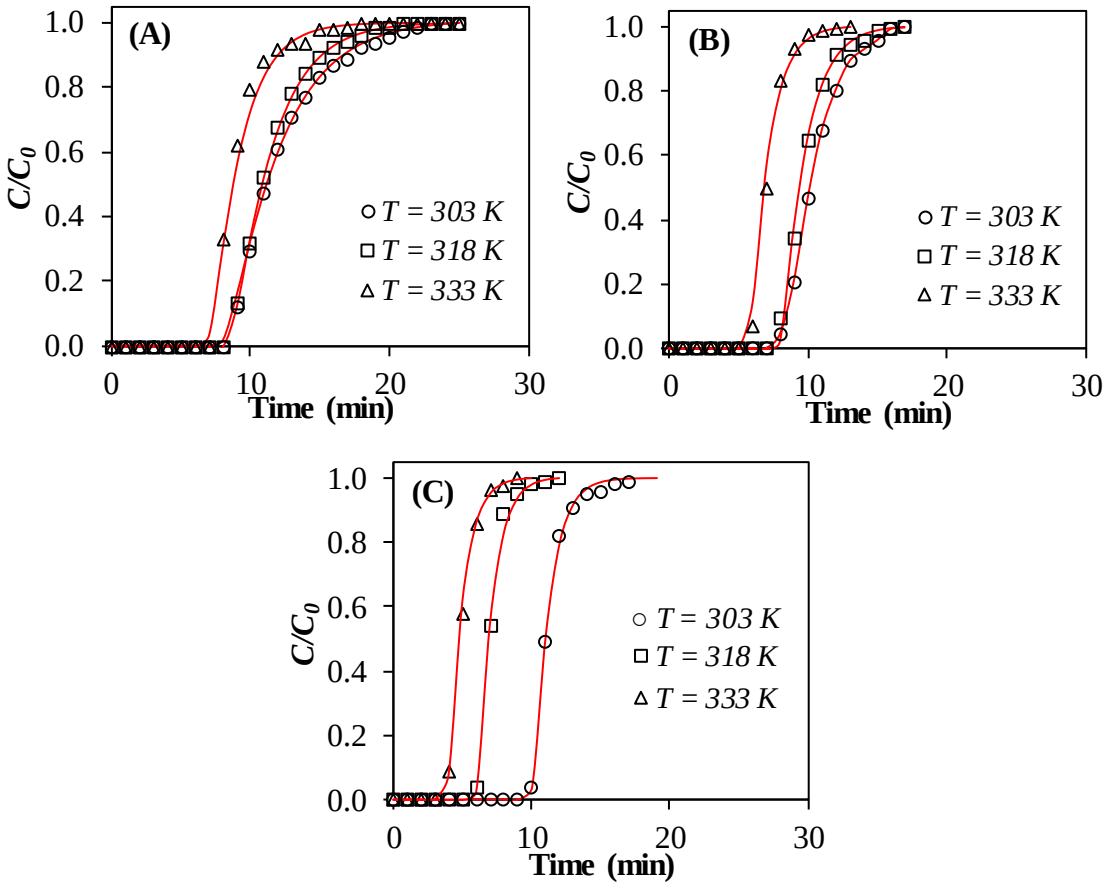

Figure 4: Breakthrough curves at different temperatures and 0.05 bar CO_2 partial pressure for SILPs with different particle size: **(A)** 500 µm, **(B)** 150 µm and **(C)** 9 µm. The red lines correspond to the LDF model implemented in Aspen Adsorption (named Lumped-Resistance model).

Figure 5A shows the values of the kinetic coefficient (k_{MTC} of Equation 2) at different temperatures for the three SILPs tested. As can be seen, these values increase while decreasing the SILP particle size, consistently with the higher gas-IL contact area. The k_{MTC} values also increase with temperature. The dependence with temperature is more pronounced at higher particle size. In fact, the breakthrough curves for the least size SILP (d_p = 9 µm,) are the steepest, close to ideal, and nearly independent of the temperature; i.e. the kinetics is so fast that the temperature hardly affects to the process within the 30 ºC range tested. In this work, we present the behavior of a SILP based on [bmim][acetate] IL, but looking at these results, it is expected that the viscosity of the IL is a key issue regarding the design of fixed-bed operations with SILPs, especially at particle sizes above 100 µm. Figure 5B represents the values of the kinetic coefficient vs the CO_2 diffusivity

(D_e) in the neat IL at each temperature, ~~as~~ obtained in previous works [15, 20, 31, 32] by the Shifflet and Yokozeki method [47]. A nearly linear relationship can be observed, suggesting that the CO_2 sorption rate in SILP is governed by the absorption phenomena in IL film, favored at lower IL viscosity (higher temperatures). The values of the kinetic coefficient at different temperatures fitted well the Arrhenius equation. Table 4 summarizes the corresponding vales of apparent activation energy and the pre-exponential factor, which will be used in later Aspen Adsorption simulations of the breakthrough curves of CO_2 capture in SILP sorbents.

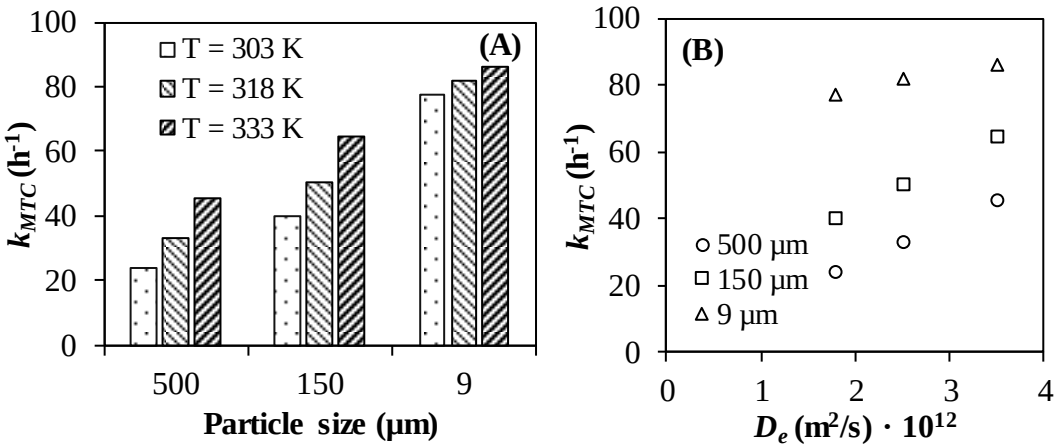

Figure 5: Values of the kinetic coefficient *(k_{MTC})* for the tested SILPs at different temperatures **(A)** and vs the CO_2 diffusivity (D_e) in the neat IL **(B)**.

Table 4: Values of the apparent activation energy and pre-exponential factor.

	SILP - 500 µm	**SILP - 150 µm**	**SILP - 9 µm**
E_a **(kJ/mol)**	17.7	13.5	3.0
k_0 **(s^{-1})**	7.62	2.35	0.07
R^2	0.993	0.990	0.999

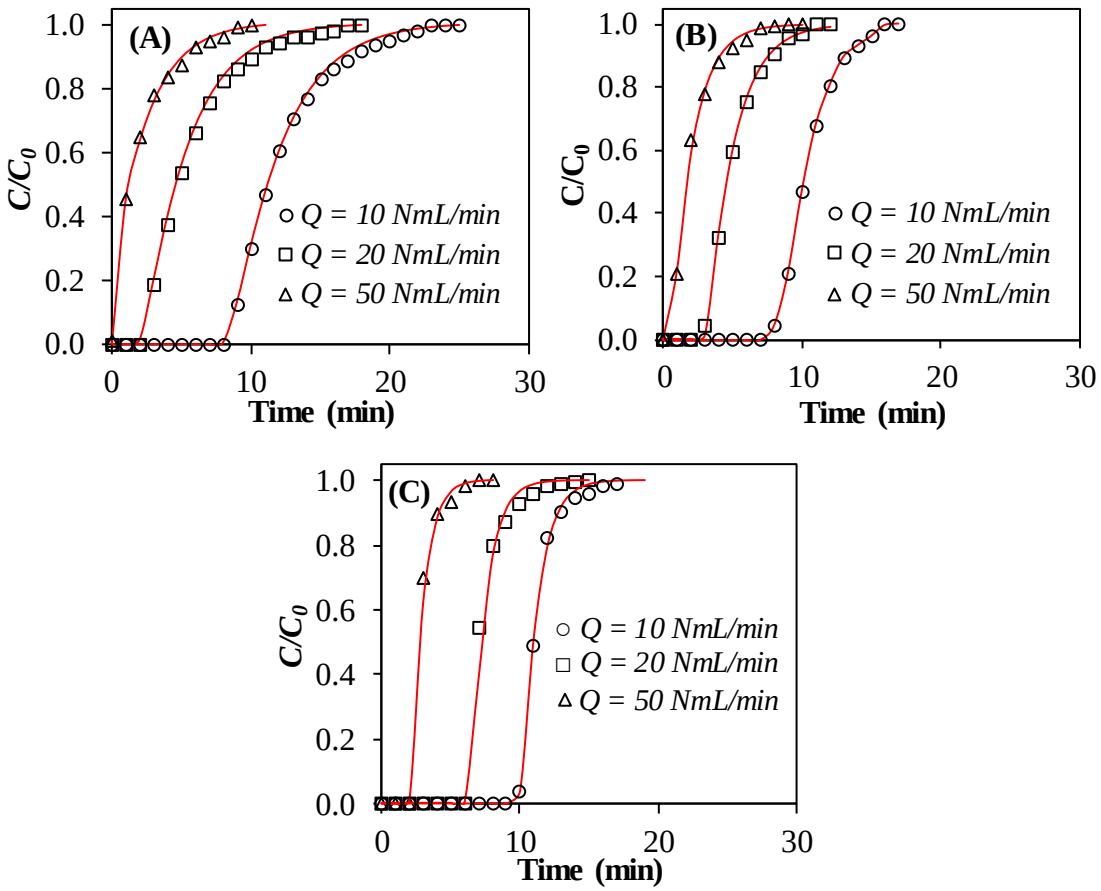

Figure 6: Breakthrough curves at different gas flow-rate for SILPs of different particle size: **(A)** 500 µm, **(B)** 150 µm and **(C)** 9 µm. [$T = 303\ K$, $p_{CO2} = 0.10\ bar$].

Figure 6 shows the breakthrough curves obtained at 303 K and 0.05 bar of CO_2 partial pressure in the inlet stream using different gas flow rates. Again, the LDF kinetic model (red lines) fits well the experimental data ($R^2 > 0.99$ in all cases). Figure 7 collects the k_{MTC} values at different gas flow-rate. Consistently with the previous conclusions, the kinetic coefficient increases when decreasing the SILP particle size, independently on the gas flow-rate. This last barely affects to k_{MTC}, indicating the absence of mass-transfer limitations in the gas-phase.

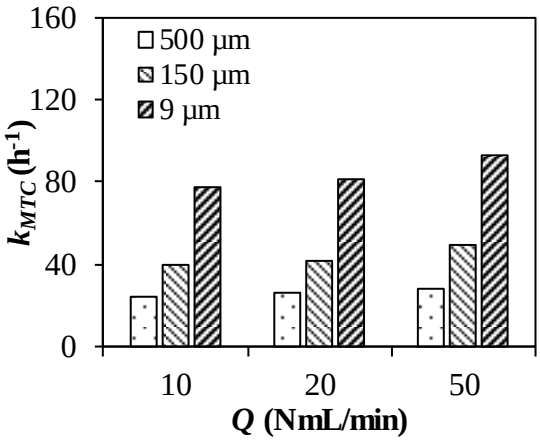

Figure 7: k_{MTC} values for SILPs at different particle size and gas flow-rate from the breakthrough curves of Figure 6. [*T = 303 K*, p_{CO2} *= 0.10 bar, P = 1 bar*].

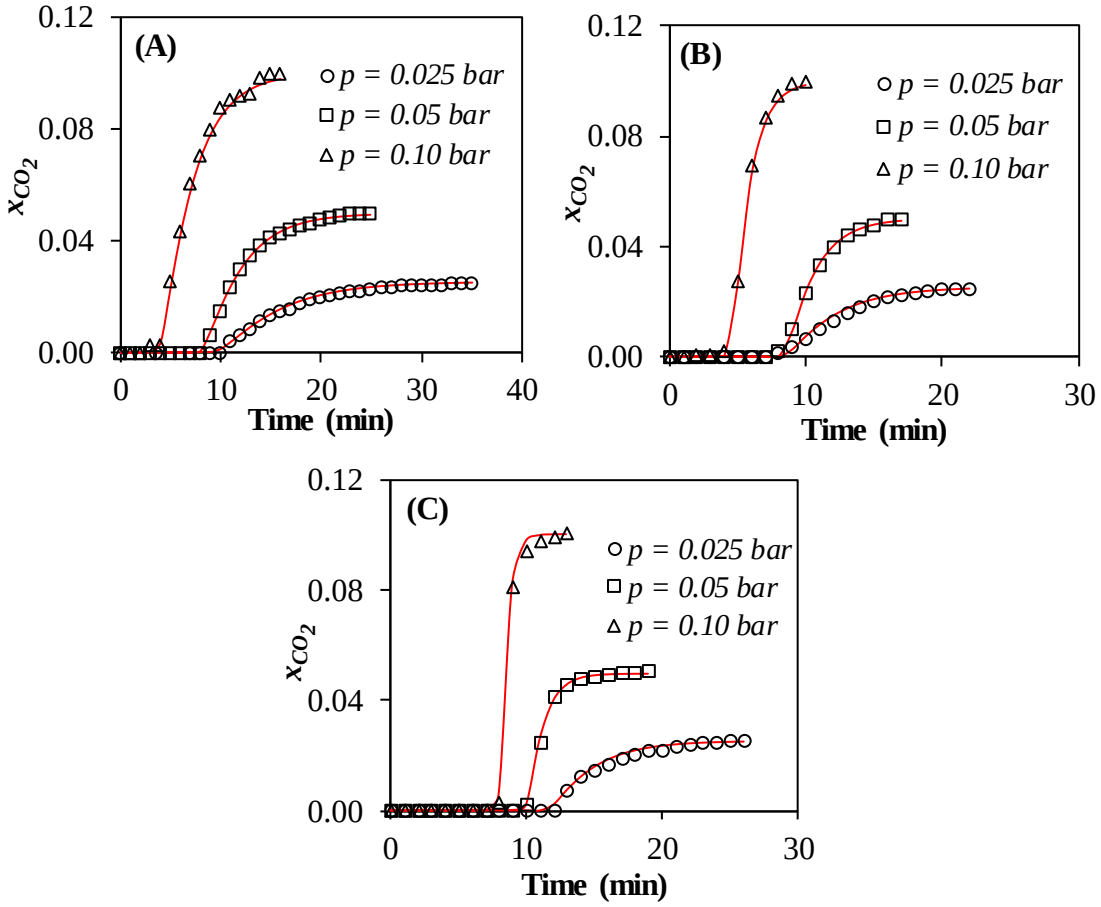

Figure 8: Breakthrough curves at different CO_2 partial pressures for the SILPs of different particle size: **(A)** 500 µm, **(B)** 150 µm and **(C)** 9 µm. *T* = 303 K; *P* = 1 atm; Gas flow-rate = 10 NmL/min.

Fixed-bed experiments at three different CO_2 inlet partial pressures (0.025, 0.05 and 0.10 bar) were carried out at 303 K, 1 atm of total pressure and 10 NmL/min gas flow rate. The results are shown in Figure 8. It is important to remark that in all cases the IL

load remained unchanged after all the CO_2 sorption tests, as confirmed by elemental analysis. The LDF kinetic model again describes well the experimental breakthrough curves ($R^2 > 0.99$ in all cases). It is clearly seen that a higher CO_2 partial pressure implies a faster sorption, consistently with the higher driving force. Figure 9 shows the values of the kinetic coefficient (k_{MTC}) at the three CO_2 partial pressures tested in the feed gas stream. It is concluded that the inlet gas CO_2 partial pressure not only determines the mass transfer driving force but significantly affects to the value of the kinetic coefficient (k_{MTC}).

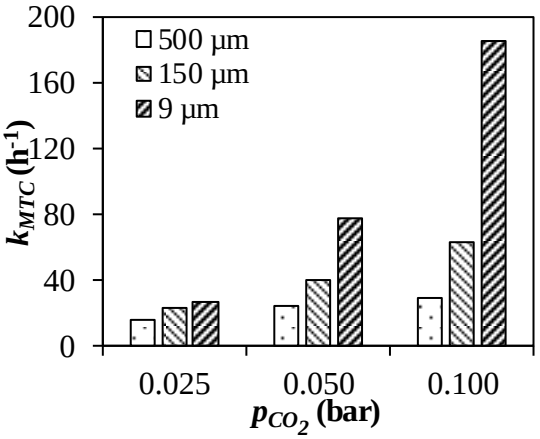

Figure 9: k_{MTC} values for SILPs of different particle sizes at three CO_2 partial pressures (see Figure for operating conditions).

Modeling CO_2 chemical sorption in fixed-bed using SILP material.

To learn more on the phenomenological aspects of the sorption process investigated, the overall resistance ($1/k_{MTC}$) was separated in two terms, according to Eq. 3, which was found to fit well the experimental results.

$$\frac{1}{k_{MTC}} = A + B \cdot \frac{r_p}{D_e} \qquad (3)$$

In that expression, r_p corresponds to the equivalent mean particle radius of the SILP and D_e was already defined as the diffusivity of CO_2 in the neat IL. Its dependence with temperature can be expressed by Equation 4 from previous experiments [31]:

$$D_e \left[\frac{m^2}{s}\right] = 3 \cdot 10^{-9} \cdot e^{-\frac{2561.55}{T}} \qquad (4)$$

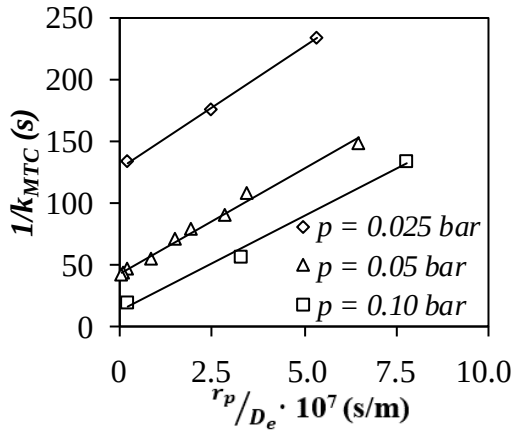

Figure 10: Fitting of Eq (3) at different CO_2 partial pressures and SILP particle size. At p_{CO2} = 0.05 bar, values at different temperatures are also included (*T* affect to D_e)

As can be seen in Figure 10, the slope of the linear relationship given by Eq. (3) is independent of the CO_2 partial pressure, while the intercept value strongly depends on it. Thus, Eq. (3) was modified into:

$$\frac{1}{k_{MTC}} = \frac{1}{1.85 \cdot p_{CO2}^{1.5}} + 2.65 \cdot 10^{-7} \cdot \frac{r_p}{3 \cdot 10^{-9} \cdot e^{-2561.55/T}} \qquad (5)$$

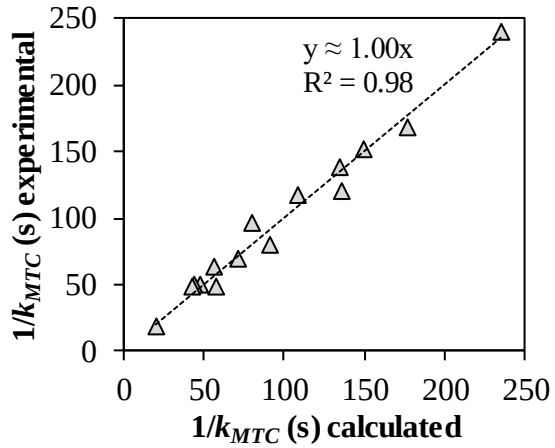

Figure 11: Validation of Eq. (5). All the experimental data of the work taken into account.

The k_{MTC} values calculated by this expression fit fairly well the experimental ones, as can be seen in Figure 11. Equation (5) considers two resistances in series. The first one, dependent of p_{CO2}, is related to the chemical absorption by the IL while the second one corresponds to CO_2 diffusion in the ionic liquid phase of the SILP.

The breakthrough curves of CO_2 sorption with the SILPs tested were simulated using Aspen Adsorption in dynamic mode within SILP particle size and CO_2 inlet partial pressure ranges wider than those tested in the experiments described so far. Figure 12 shows the resulting curves at 303 K.

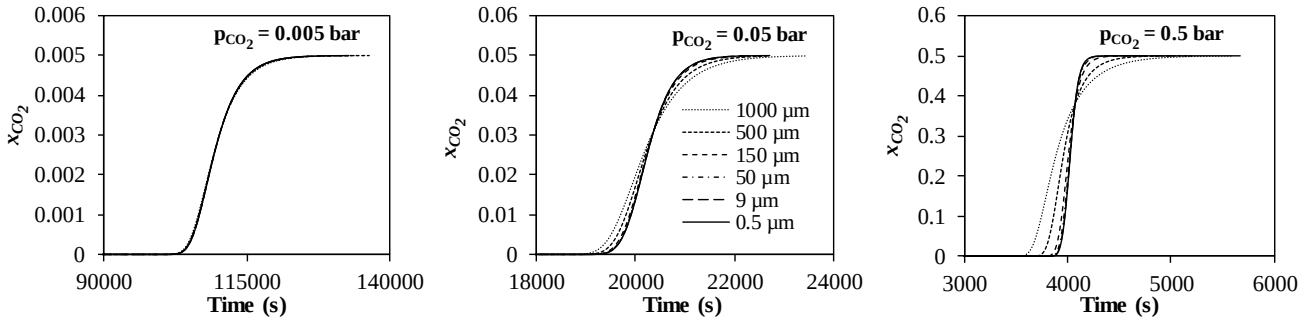

Figure 12: Breakthrough curves of CO_2 sorption in fixed-bed calculated by Aspen Adsorption in dynamic mode for different SILP particle sizes and CO_2 partial pressures (T = 303 K).

The curves become steeper at increasing CO_2 partial pressure. Regarding the effect of SILP particle size, it strongly depends on the inlet CO_2 partial pressure. At very low CO_2 partial pressure, the SILP particle size does not affect the kinetics of the process, having almost the same curve shape in all cases. At higher p_{CO2} values, the length of the mass-transfer zone becomes shorter as the SILP particle size decreases, being the effect more pronounced at increasing p_{CO2}. These results indicate the existence of different rate control regimes depending on the operating range of these two variables. At very low CO_2 partial pressure, the rate of the process is governed by the chemical reaction determining CO_2 sorption, while as p_{CO2} increases so does the reaction rate and the CO_2 diffusion in the IL turns to be the controlling step.

CO_2 capture would commonly be carried out from gas streams with a relative concentration of this component well above the limit when mass-transfer control already occurs and, therefore, the SILP particle size is an important issue to be considered for a cost-effective use of this type of sorbent. A balance between the effective bed sorption capacity at the established breaking point and the gas pressure loss, depending on the particle size of the sorbent material, must be optimized. In principle, looking at the breakthrough curves at high and intermediate $p_{CO2,}$ a SILP particle size somewhere in the range of 0.15 to 0.5 mm seems to be the most reasonable. Further research is addressed toward this main question regarding potential application of these SILPs for CO_2 capture upon fixed bed sorption.

Conclusions

SILP material with remarkably different particle sizes, based on the IL 1-butyl-3-methylimidazolium acetate, was evaluated in detail as CO_2 sorbents. The prepared SILP material was characterized by SEM, porous texture, thermal stability, and elemental composition. The gravimetric measurements at three different temperatures show that the CO_2 sorption capacity is only attributed to the IL. The CO_2 sorption isotherms were successfully fitted to the Langmuir-Freundlich model implemented in Aspen Adsorption. The effect of the SILP particle size, temperature, gas flow-rate and CO_2 partial pressure was evaluated in fixed-bed experiments. The different breakthrough curves were successfully fitted using Aspen Adsorption to a linear driving force model, allowing to obtain the effective overall kinetic coefficient k_{MTC}. The k_{MTC} values revealed that the CO_2 sorption rate increases when decreasing the SILP particle size and increasing the temperature. The gas flow-rate does not have any noticeable effect on the mass transfer rate in the range investigated. The increase in the p_{CO2} presents a remarkable effect on the sorption rate. The results suggest that at very low p_{CO2} the chemical absorption is the controlling step while as that partial pressure increases, CO_2 diffusion in the IL phase of SILP turns to be the governing stage. Aspen Adsorption simulator was used to evaluate the SILP behavior within particle size and CO_2 inlet partial pressure covering wider ranges than those tested in the experimental runs. Depending on inlet CO_2 partial pressure, it was found a remarkably different effect of particle size on SILP sorbent performance, because of the shift of control regime from chemical absorption to CO_2 diffusion in the IL. This methodology allows optimizing the operation at given conditions of temperature and $p_{CO2,}$ by selecting the type of IL and SILP particle size.

Supporting Information

Detailed information of the isotherm models used and the additional Aspen Adsorption input required to simulate in dynamic mode that was not described on the paper. N_2 adsorption/desorption isotherms @ 77K of empty silica particles of three different sizes. TGA analysis of empty silica and prepared SILP materials. Comparison of CO_2 sorption capacity of pure IL and SILP materials. CO_2 adsorption blank experiment with empty SiO_2

Acknowledgments

The authors are very grateful to Ministerio de Economía y Competitividad (MINECO) of Spain (project CTQ2017-89441-R) and Comunidad de Madrid (P2018/EMT4348) for financial support and Centro de Computación Científica de la Universidad Autónoma de Madrid for computational facilities.

References

1. Plasseraud, L., *Carbon Dioxide as Chemical Feedstock. Edited by Michele Aresta*. 2010; Vol. 3, p 631-632. DOI 10.1002/cssc.201000097
2. Hatzigeorgiou, E.; Polatidis, H.; Haralambopoulos, D., Energy CO_2 Emissions for 1990–2020: A Decomposition Analysis for EU-25 and Greece. *Energy Sources, Part A: Recovery, Utilization, and Environmental Effects* **2010,** *32* (20), 1908-1917. DOI 10.1080/15567030902937101
3. Baena-Moreno, F. M.; Rodríguez-Galán, M.; Vega, F.; Alonso-Fariñas, B.; Vilches Arenas, L. F.; Navarrete, B., Carbon capture and utilization technologies: a literature review and recent advances. *Energy Sources, Part A: Recovery, Utilization, and Environmental Effects* **2019,** *41* (12), 1403-1433. DOI 10.1080/15567036.2018.1548518
4. Bui, M.; Adjiman, C. S.; Bardow, A.; Anthony, E. J.; Boston, A.; Brown, S.; Fennell, P. S.; Fuss, S.; Galindo, A.; Hackett, L. A.; Hallett, J. P.; Herzog, H. J.; Jackson, G.; Kemper, J.; Krevor, S.; Maitland, G. C.; Matuszewski, M.; Metcalfe, I. S.; Petit, C.; Puxty, G.; Reimer, J.; Reiner, D. M.; Rubin, E. S.; Scott, S. A.; Shah, N.; Smit, B.; Trusler, J. P. M.; Webley, P.; Wilcox, J.; Mac Dowell, N., Carbon capture and storage (CCS): the way forward. *Energ. Environ. Sci.* **2018,** *11* (5), 1062-1176. DOI 10.1039/C7EE02342A
5. Gaurina-Medimurec, N.; Novak-Mavar, K.; Majic, M., Carbon Capture and Storage (CCS): Technology, Projects and Monitoring Review. *Rudarsko-Geolosko-Naftni Zbornik* **2018,** *33* (2), 1-15. DOI 10.17794/rgn.2018.2.1
6. Amaral, M.; Crespo, E. A.; Dariva, C.; Vega, L. F.; Carvalho, P. J.; Coutinho, J. A. P., High-pressure solubility of CO_2 in glymes. *Fuel* **2018,** *219*, 120-125. DOI 10.1016/j.fuel.2018.01.084
7. Jaramillo, P.; Griffin, W. M.; McCoy, S. T., Life Cycle Inventory of CO_2 in an Enhanced Oil Recovery System. *Energ. Environ. Sci.* **2009,** *43* (21), 8027-8032. DOI 10.1021/es902006h
8. Xu, Y.; P. Schutte, R.; G. Hepler, L., Solubilities of Carbon Dioxide, Hydrogen Sulfide and Sulfur Dioxide in Physical Solvents. 1992; Vol. 70, p 569-573. DOI 10.1002/cjce.5450700321
9. Fillion, J. J.; Bennett, J. E.; Brennecke, J. F., The Viscosity and Density of Ionic Liquid + Tetraglyme Mixtures and the Effect of Tetraglyme on CO_2 Solubility. *J. Chem. Eng. Data* **2017,** *62* (2), 608-622. DOI 10.1021/acs.jced.6b00596
10. Jones, C. W., CO_2 Capture from Dilute Gases as a Component of Modern Global Carbon Management. *Annual Review of Chemical and Biomolecular Engineering* **2011,** *2* (1), 31-52. DOI 10.1146/annurev-chembioeng-061010-114252
11. Papatryfon, X. L.; Heliopoulos, N. S.; Molchan, I. S.; Zubeir, L. F.; Bezemer, N. D.; Arfanis, M. K.; Kontos, A. G.; Likodimos, V.; Iliev, B.; Romanos, G. E.; Falaras, P.; Stamatakis, K.; Beltsios, K. G.; Kroon, M. C.; Thompson, G. E.; Klöckner,

J.; Schubert, T. J. S., CO_2 Capture Efficiency, Corrosion Properties, and Ecotoxicity Evaluation of Amine Solutions Involving Newly Synthesized Ionic Liquids. *Ind. Eng. Chem. Res.* **2014,** *53* (30), 12083-12102. DOI 10.1021/ie501897d
12. Rogers, R. D.; Seddon, K. R., Ionic Liquids--Solvents of the Future? *Science* **2003,** *302* (5646), 792-793. DOI 10.1126/science.1090313
13. Earle, M.; Seddon, K., Ionic liquids. Green solvents for the future. 2002; Vol. 72, pp 10-25.
14. Welton, T., Ionic liquids: a brief history. *Biophys. Rev.* **2018,** *10* (3), 691-706. DOI 10.1007/s12551-018-0419-2
15. Moya, C.; Palomar, J.; Gonzalez-Miquel, M.; Bedia, J.; Rodriguez, F., Diffusion Coefficients of CO_2 in Ionic Liquids Estimated by Gravimetry. *Ind. Eng. Chem. Res.* **2014,** *53* (35), 13782-13789. DOI 10.1021/ie501925d
16. Saravanamurugan, S.; Kunov-Kruse, A. J.; Fehrmann, R.; Riisager, A., Amine-Functionalized Amino Acid- based Ionic Liquids as Efficient and High- Capacity Absorbents for CO_2. *Chemsuschem* **2014,** *7* (3), 897-902. DOI 10.1002/cssc.201300691
17. Aghaie, M.; Rezaei, N.; Zendehboudi, S., A systematic review on CO_2 capture with ionic liquids: Current status and future prospects. *Renew. Sust. Energ. Rev.* **2018,** *96*, 502-525. DOI 10.1016/j.rser.2018.07.004
18. Carvalho, P. J.; Kurnia, K. A.; Coutinho, J. A. P., Dispelling some myths about the CO_2 solubility in ionic liquids. *Phys. Chem. Chem. Phys.* **2016,** *18* (22), 14757-14771. DOI 10.1039/C6CP01896C
19. Seo, S.; Quiroz-Guzman, M.; DeSilva, M. A.; Lee, T. B.; Huang, Y.; Goodrich, B. F.; Schneider, W. F.; Brennecke, J. F., Chemically Tunable Ionic Liquids with Aprotic Heterocyclic Anion (AHA) for CO_2 Capture. *J. Phys. Chem. B* **2014,** *118* (21), 5740-5751. DOI 10.1021/jp502279w
20. Palomar, J.; Larriba, M.; Lemus, J.; Moreno, D.; Santiago, R.; Moya, C.; de Riva, J.; Pedrosa, G., Demonstrating the key role of kinetics over thermodynamics in the selection of ionic liquids for CO_2 physical absorption. *Sep. Purif. Technol.* **2019,** *213*, 578-586. DOI 10.1016/j.seppur.2018.12.059
21. Goodrich, B. F.; de la Fuente, J. C.; Gurkan, B. E.; Lopez, Z. K.; Price, E. A.; Huang, Y.; Brennecke, J. F., Effect of Water and Temperature on Absorption of CO_2 by Amine-Functionalized Anion-Tethered Ionic Liquids. *J. Phys. Chem. B.* **2011,** *115* (29), 9140-9150. DOI 10.1021/jp2015534
22. Mota-Martinez, M. T.; Brandl, P.; Hallett, J. P.; Mac Dowell, N., Challenges and opportunities for the utilisation of ionic liquids as solvents for CO_2 capture. *Mol. Syst. Des. Eng.* **2018,** *3* (3), 560-571. DOI 10.1039/C8ME00009C
23. Leclaire, J.; Heldebrant, D. J., A call to (green) arms: a rallying cry for green chemistry and engineering for CO_2 capture, utilisation and storage. *Green Chem.* **2018,** *20* (22), 5058-5081. DOI 10.1039/C8GC01962B
24. Kolding, H.; Fehrmann, R.; Riisager, A., CO_2 Capture technologies: Current status and new directions using supported ionic liquid phase (SILP) absorbers. *Sci. China-Chem.* **2012,** *55* (8), 1648-1656. DOI 10.1007/s11426-012-4683-x
25. Riisager, A.; Flicker, S.; Haumann, M.; Wasserscheid, P.; Fehrmann, R., Supported Ionic Liquid-Phase (Silp) Catalysts in Continuous Flow Processes. 2004; Vol. 2004-24, p 630-638. DOI 10.1149/200424.0630PV
26. Romanos, G. E.; Schulz, P. S.; Bahlmann, M.; Wasserscheid, P.; Sapalidis, A.; Katsaros, F. K.; Athanasekou, C. P.; Beltsios, K.; Kanellopoulos, N. K., CO_2 Capture by Novel Supported Ionic Liquid Phase Systems Consisting of Silica Nanoparticles Encapsulating Amine-Functionalized Ionic Liquids. *J. Phys. Chem. C.* **2014,** *118* (42), 24437-24451. DOI 10.1021/jp5062946

27. Balsamo, M.; Erto, A.; Lancia, A.; Totarella, G.; Montagnaro, F.; Turco, R., Post-combustion CO_2 capture: On the potentiality of amino acid ionic liquid as modifying agent of mesoporous solids. *Fuel* **2018,** *218*, 155-161. DOI 10.1016/j.fuel.2018.01.038
28. Lemus, J.; Palomar, J.; Gilarranz, M.; J. Rodriguez, J., Characterization of Supported Ionic Liquid Phase (SILP) materials prepared from different supports. 2011; Vol. 17, p 561-571. DOI: 10.1007/s10450-011-9327-5
29. Palomar, J.; Lemus, J.; Alonso-Morales, N.; Bedia, J.; Gilarranz, M. A.; Rodriguez, J. J., Encapsulated ionic liquids (ENILs): from continuous to discrete liquid phase. *Chem. Commun.* **2012,** *48* (80), 10046-10048. DOI 10.1039/C2CC35291E
30. Moya, C.; Alonso-Morales, N.; de Riva, J.; Morales-Collazo, O.; Brennecke, J. F.; Palomar, J., Encapsulation of Ionic Liquids with an Aprotic Heterocyclic Anion (AHA-IL) for CO_2 Capture: Preserving the Favorable Thermodynamics and Enhancing the Kinetics of Absorption. *J. Phys. Chem. B.* **2018,** *122* (9), 2616-2626. DOI 10.1021/acs.jpcb.7b12137
31. Moya, C.; Alonso-Morales, N.; Gilarranz, M. A.; Rodriguez, J. J.; Palomar, J., Encapsulated Ionic Liquids for CO_2 Capture: Using 1-Butyl-methylimidazolium Acetate for Quick and Reversible CO_2 Chemical Absorption. *ChemPhysChem* **2016,** *17* (23), 3891-3899. DOI 10.1002/cphc.201600977
32. Santiago, R.; Lemus, J.; Moreno, D.; Moya, C.; Larriba, M.; Alonso-Morales, N.; Gilarranz, M. A.; Rodríguez, J. J.; Palomar, J., From kinetics to equilibrium control in CO_2 capture columns using Encapsulated Ionic Liquids (ENILs). *Chem. Eng. J.* **2018,** *348*, 661-668. DOI 10.1016/j.cej.2018.05.029
33. Santiago, R.; Lemus, J.; Moya, C.; Moreno, D.; Alonso-Morales, N.; Palomar, J., Encapsulated Ionic Liquids to Enable the Practical Application of Amino Acid-Based Ionic Liquids in CO_2 Capture. *ACS Sustain. Chem. Eng.* **2018,** *6* (11), 14178-14187. DOI 10.1021/acssuschemeng.8b02797
34. Lemus, J.; Bedia, J.; Moya, C.; Alonso-Morales, N.; Gilarranz, M.; Palomar, J.; J Rodriguez, J., Ammonia Capture from Gas Phase by Encapsulated Ionic Liquids (ENILs). 2016; Vol. 6. DOI 10.1039/C6RA11685J
35. Mota-Martinez, M. T.; Brandl, P.; Hallett, J. P.; Mac Dowell, N., Challenges and for the utilisation of ionic liquids as solvents for CO_2 capture. *Mol. Syst. Des. Eng.* **2018,** *3* (3), 560-571. DOI 10.1039/C8ME00009C
36. Ben-Mansour, R.; Habib, M. A.; Bamidele, O. E.; Basha, M.; Qasem, N. A. A.; Peedikakkal, A.; Laoui, T.; Ali, M., Carbon capture by physical adsorption: Materials, experimental investigations and numerical modeling and simulations - A review. *Appl. Energy* **2016,** *161*, 225-255. DOI 10.1016/j.apenergy.2015.10.011
37. Rashidi, N. A.; Yusup, S., An overview of activated carbons utilization for the post-combustion carbon dioxide capture. *J. CO_2 Util.* **2016,** *13*, 1-16. DOI 10.1016/j.jcou.2015.11.002
38. Wang, J. Y.; Huang, L.; Yang, R. Y.; Zhang, Z.; Wu, J. W.; Gao, Y. S.; Wang, Q.; O'Hare, D.; Zhong, Z. Y., Recent advances in solid sorbents for CO_2 capture and new development trends. *Energy Environ. Sci.* **2014,** *7* (11), 3478-3518. DOI 10.1039/C4EE01647E
39. Balsamo, M.; Rodríguez-Reinoso, F.; Montagnaro, F.; Lancia, A.; Erto, A., Highlighting the Role of Activated Carbon Particle Size on CO_2 Capture from Model Flue Gas. *Ind. Eng. Chem. Res.* **2013,** *52* (34), 12183-12191. DOI 10.1021/ie4018034
40. Dadwhal, M.; Kim, T. W.; Sahimi, M.; Tsotsis, T. T., Study of CO_2 Diffusion and Adsorption on Calcined Layered Double Hydroxides: The Effect of Particle Size. *Ind. Eng. Chem. Res.* **2008,** *47* (16), 6150-6157. DOI 10.1021/ie701701d

41. Gatti, G.; Vittoni, C.; Costenaro, D.; Paul, G.; Mangano, E.; Brandani, S.; Marchese, L.; Bisio, C., The influence of particle size of amino-functionalized MCM-41 silicas on CO_2 adsorption. *Phys. Chem. Chem. Phys.* **2017,** *19* (43), 29449-29460. DOI 10.1039/C7CP05177H
42. Mastalerz, M.; Hampton, L.; Drobniak, A.; Loope, H., Significance of analytical particle size in low-pressure N_2 and CO_2 adsorption of coal and shale. *Int. J. Coal Geol.* **2017,** *178*, 122-131. DOI 10.1016/j.coal.2017.05.003
43. Bhatt, T. S.; Sliepcevich, A.; Storti, G.; Rota, R., Experimental and Modeling Analysis of Dual-Reflux Pressure Swing Adsorption Process. *Ind. Eng. Chem. Res.* **2014,** *53* (34), 13448-13458. DOI 10.1021/ie502057k
44. Bhatt, T. S.; Storti, G.; Rota, R., Detailed simulation of dual-reflux pressure swing adsorption process. *Chem. Eng. Sci.* **2015,** *122*, 34-52. DOI 10.1016/j.ces.2014.09.013
45. Santos, M. G. R. S.; Correia, L. M. S.; de Medeiros, J. L.; Araujo, O. d. Q. F., Natural gas dehydration by molecular sieve in offshore plants: Impact of increasing carbon dioxide content. *Energy Convers. Manag.* **2017,** *149*, 760-773. DOI 10.1016/j.enconman.2017.03.005
46. Lei, Z.; Dai, C.; Chen, B., Gas Solubility in Ionic Liquids. *Chem. Rev.* **2014,** *114* (2), 1289-1326. DOI 10.1021/cr300497a
47. Shiflett, M. B.; Yokozeki, A., Solubilities and Diffusivities of Carbon Dioxide in Ionic Liquids: [bmim][PF_6] and [bmim][BF_4]. *Ind. Eng. Chem. Res.* **2005,** *44* (12), 4453-4464. DOI 10.1021/ie058003d

For Table of Contents Use Only

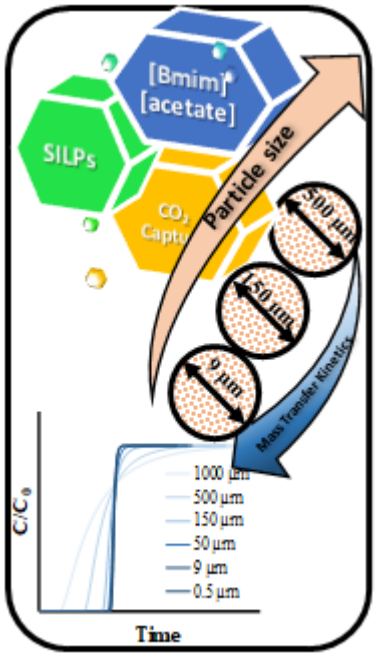

Design of CO_2 capture operation in fixed-bed with SILPs optimizing the particle size